ISSN 1392-1207. MECHANIKA. Vol. 31, No. 1, 2025: 73–79

The Improvement of Detection Precision of Internal Surface Detection System of Main Cylinder

Guilong WANG*, Bo YU**
**School of Innovation and Entrepreneurship Education for College Students, Changchun Institute of Technology, Changchun 130012, Jilin, China, E-mail: jd_wgl@ccit.edu.cn*
***School of Mechanical and Electrical Engineering, Changchun Institute of Technology, Changchun 130012, Jilin, China, E-mail: jd_yb@ccit.edu.cn (Corresponding Author)*
https://doi.org/10.5755/j02.mech.38800

1. Introduction

With the rapid development of our country's economy, the automobile industry has also been unprecedented development opportunities, car ownership has increased significantly, followed by the issue of car safety. According to the statistic analysis, the main cylinder of the automobile brake system is the key component which affects the automobile brake performance, and the inspection quality of its inner surface is especially important, which is one of the essential inspection items before leaving the factory [1].

At present, the method of measuring the inner surface of brake master cylinder mainly depends on manual operation for contact measurement, and its detection performance and accuracy can not meet the current needs of modernization and industrial production [2, 3]. Therefore, it is urgent to develop a high-precision and high-efficiency brake master cylinder internal surface detection system using advanced detection technology.

In view of the fact that the current inspection technology of the inner surface of the main cylinder of the brake is backward, an advanced inspection scheme integrating light, machine, electricity and calculation is put forward, and a test prototype is developed, this method effectively solves the problem of measuring precision and efficiency of internal surface of master cylinder.

2. Detection System Analysis

Fig. 1 shows the brake master cylinder surface inspection system structure diagram. The image of the compensating hole is output by the endoscope system and CCD technology, and the position of the compensating hole is output by grating detection technology.

As can be seen from Fig. 1, the detection system consists of a vertical linear axis z and a horizontal rotary axis C.

3. Error Analysis

The error element of the detection system is caused by the undesired component of the relative motion of the structural components, which directly affects the detection accuracy of the detection system. From the analysis of the overall operation of the detection system, it is known that the thermal deformation error and the error of the combined force can be neglected, and the geometric error is the key factor affecting the detection accuracy [4, 5]. Therefore, to realize high quality and high efficiency on-line detection of the detection system, the geometric error elements should be analyzed in detail.

Any linear axis of motion has six geometric errors [6, 7], as shown in Fig. 2: $\delta_x(x)$, $\delta_y(x)$, $\delta_z(x)$, $\varepsilon_x(x)$, $\varepsilon_y(x)$, $\varepsilon_z(x)$.

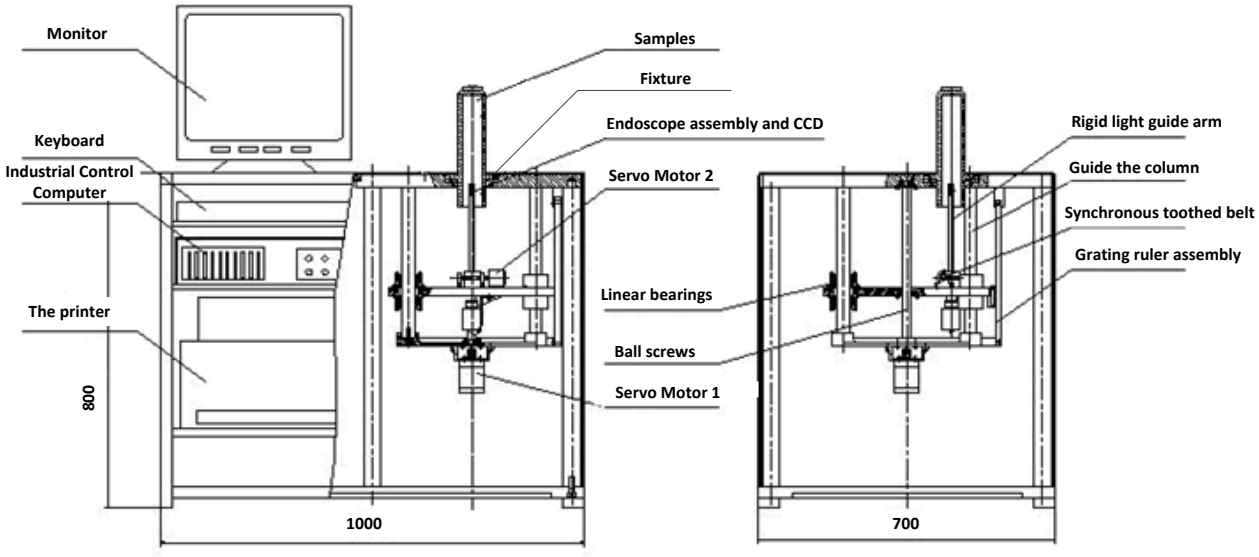

Fig. 1 Schematic diagram of detection system

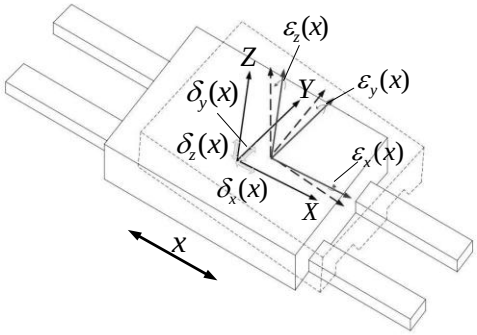

Fig. 2 Geometric error diagram of linear motion axis

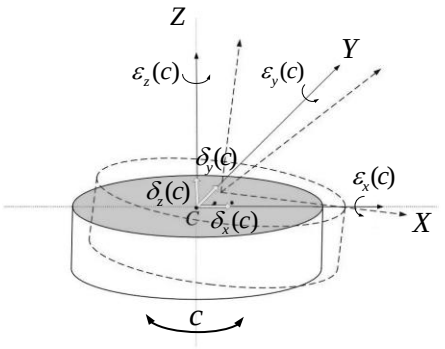

Fig. 3 Geometrical error diagram of rotating shaft

Therefore, the vertical linear axis Z of the detection system should have six geometric errors: $\delta_x(c)$, $\delta_y(c)$, $\delta_z(c)$, $\varepsilon_x(c)$, $\varepsilon_y(c)$, $\varepsilon_z(c)$.

Similarly, there are six geometric errors [8, 9] for any axis of rotation, as shown in Fig. 3: $\delta_x(c)$, $\delta_y(c)$, $\delta_z(c)$, $\varepsilon_x(c)$, $\varepsilon_y(c)$, $\varepsilon_z(c)$. And there are six geometric errors in the horizontal axis C of the measuring system: $\Delta X(C)$, $\Delta Y(C)$, $\delta z(C)$, $\varepsilon x(C)$, $\varepsilon y(C)$, $\varepsilon z(C)$.

In addition, there is a verticality error between the vertical linear axis Z and the horizontal rotary axis C: η_{ZC}. Therefore, the detection system should have 13 geometric errors.

4. Error Modeling

Multi-body system is a kind of complex mechanical system in which multiple rigid bodies are combined in some connecting form. The error modeling technology based on multi-body system has the advantages of strong generality and good systematicness [10] , based on the theory of multi-body system, the error model of detection system is built, as follows.

4.1. Topology and low order volume array

According to the structure of the motion chain of the detection system, it can be divided into:

1) Detecting motion chain, endoscope assembly (N)→ vertical translational axis (Z)→ Bracket-1(P_1)→ fuselage (R);

2) Workpiece motion chain: fuselage (R) < Bracket-2(P_2) < horizontal axis of rotation (C) < calibration block (J) < measured part (M).

The existing topology and low-void array structure are shown in Fig. 4 and Table 1.

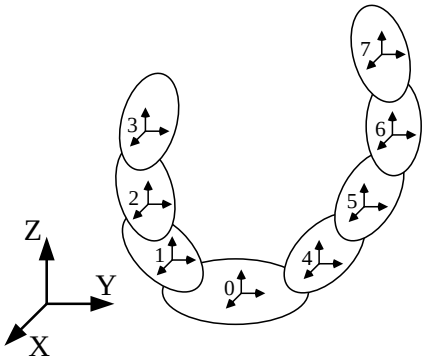

Fig. 4 Topology: *0* – fuselage, *1* – brackets-1, *2* – vertical translational axis, *3* – endoscopic components, *4* – brackets-2, *5* – horizontal axis of rotation, *6* – calibration block, *7* – to be tested

Table 1

Low-order volume array

Typical (j)	*0*	*1*	*2*	*3*	*4*	*5*	*6*	*7*
$L^0(j)$	0	1	2	3	4	5	6	7
$L^1(j)$	-	0	1	2	3	0	5	6
$L^2(j)$	-	-	0	1	2	-	0	5
$L^3(j)$	-	-	-	0	1	-	-	0
$L^4(j)$	-	-	-	-	0	-	-	-

4.2. Set the coordinate system

The unified coordinate system should be established firstly for motion modeling based on multi-body system theory. When the coordinate system is set up, all components are regarded as individual, and sub-coordinate system is set in the individual, the original origin and the original coordinate axis are same and overlap. Assuming that the body coordinates of the initial state detection system are O_R, the O_J, O_Z, O_{P1}, O_{P2}, O_C coordinates are set to be the same as the O_R initial point, and the axes overlap Set the O_N to be the same as the O_M initial point, with the axes overlapping, and the O_N initial point in O_R with the coordinates (D_x, D_y, D_z) , as shown in Fig. 5, coordinate system right subscript letters -LRB-detection system structural parts name) for its specific attribution.

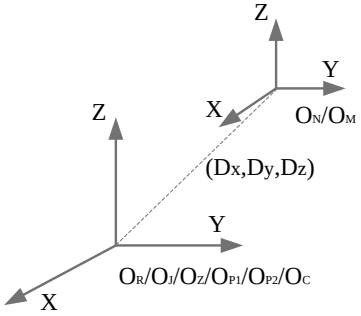

Fig. 5 Coordinate system settings

4.3. Establish the ideal transformation matrix

According to the theory of multi-body system, the degree of freedom between the parts of the detection system is analyzed, and the ideal transformation matrix is established as shown in Table 2, in which $I_{4\times4}$ is the unit matrix of order 4.

Under the ideal condition, the detection point of endoscope and the detection point of the object under test coincide. The homogeneous coordinates of the detection point of endoscope in the coordinate system O_N are: o_t=[0 0 0 1]^T, according to the theory of multi-body system, the zero-order motion equation of the endoscopic detection point in the coordinate O_M can be established, as shown in Eq. (1).

$$o_w = \left[T_{04}T_{45}T_{56}T_{67}\right]^{-1}\left[T_{01}T_{12}T_{23}\right]\cdot o_t . \tag{1}$$

In Eq. (1), $T_{ij}=T_{ijp}\cdot T_{ijs}$, T_{ijp} is the static transformation matrix, T_{ijs} is the motion transformation matrix.

Table 2

Ideal change matrix

Components	Still transformation matrix	Motion transformation matrix
0(R)	$T_{00p}=I_{4\times4}$	$T_{00s}=I_{4\times4}$
1(P_1)	$T_{01p}=I_{4\times4}$	$T_{01s}=I_{4\times4}$
2(Z)	$T_{12p}=I_{4\times4}$	$T_{12s}=\begin{bmatrix}1&0&0&0\\0&1&0&0\\0&0&1&z\\0&0&0&1\end{bmatrix}$
3(N)	$T_{23p}=\begin{bmatrix}1&0&0&D_x\\0&1&0&D_y\\0&0&1&D_z\\0&0&0&1\end{bmatrix}$	$T_{23s}=I_{4\times4}$
4(P_2)	$T_{04p}=I_{4\times4}$	$T_{04s}=I_{4\times4}$
5(C)	$T_{45p}=I_{4\times4}$	$T_{45s}=\begin{bmatrix}\cos C&-\sin C&0&0\\\sin C&\cos C&0&0\\0&0&1&0\\0&0&0&1\end{bmatrix}$
6(J)	$T_{56p}=I_{4\times4}$	$T_{56s}=I_{4\times4}$
7(M)	$T_{67p}=\begin{bmatrix}1&0&0&D_x\\0&1&0&D_y\\0&0&1&D_z\\0&0&0&1\end{bmatrix}$	$T_{67s}=I_{4\times4}$

4.4. Integrated error modeling

In the practical work of the detection system, due to the existence of geometric error, the detection point of the endoscope deviates from the theoretical detection point of the object to produce detection error. According to the geometric error analysis, the comprehensive error model of the detection system is established, which can reflect the influence of the detection accuracy of the detection system.

1. O_N coordinate system

Due to the installation error of endoscope N on lead screw component t: Δx_N, Δy_N, Δz_N, $\Delta\alpha_N$, $\Delta\beta_N$, $\Delta\gamma_N$, the actual transformation matrix of O_N coordinate system relative to O_T coordinate system is:

$$\begin{cases} T_{34p}' = \begin{bmatrix} 1 & -\Delta\gamma_N & \Delta\beta_N & \Delta x_N \\ \Delta\gamma_N & 1 & -\Delta\alpha_N & \Delta y_N \\ -\Delta\beta_N & \Delta\alpha_N & 1 & \Delta z_N \\ 0 & 0 & 0 & 1 \end{bmatrix} \\ T_{34s}' = I_{4\times4} \end{cases}. \tag{2}$$

2. O_Z coordinate system

According to the previous analysis, there should be six errors in the detection process of the vertical linear axis Z: $\delta_x(Z)$, $\delta_y(Z)$, $\delta_z(Z)$, $\varepsilon_x(Z)$, $\varepsilon_y(Z)$, $\varepsilon_z(Z)$. Thus, the actual motion transformation matrix of the O_Z coordinate system relative to the O_{P1} coordinate system is:

$$\begin{cases} T_{12p}' = I_{4\times4} \\ T_{12s}' = \begin{bmatrix} 1 & -\varepsilon_z(Z) & \varepsilon_y(Z) & \delta_x(Z) \\ \varepsilon_z(Z) & 1 & -\varepsilon_x(Z) & \delta_y(Z) \\ -\varepsilon_y(Z) & \varepsilon_x(Z) & 1 & z+\delta_z(Z) \\ 0 & 0 & 0 & 1 \end{bmatrix} \end{cases}. \tag{3}$$

3. O_{P1} coordinate system

The actual transformation matrix of O_{P1} coordinate system relative to O_R coordinate system is: Δx_{p1}, Δy_{p1}, Δz_{p1}, $\Delta\alpha_{p1}$, $\Delta\beta_{p1}$, $\Delta\gamma_{p1}$:

$$\begin{cases} T_{01p}' = \begin{bmatrix} 1 & -\Delta\gamma_{P1} & \Delta\beta_{P1} & \Delta x_{P1} \\ \Delta\gamma_{P1} & 1 & -\Delta\alpha_{P1} & \Delta y_{P1} \\ -\Delta\beta_{P1} & \Delta\alpha_{P1} & 1 & \Delta z_{P1} \\ 0 & 0 & 0 & 1 \end{bmatrix} \\ T_{01s}' = I_{4\times4} \end{cases}. \tag{4}$$

4. O_R coordinate system

The generalized coordinate system is established with reference to the fuselage, so the O_R coordinate system has no error.

5. O_{P2} coordinate system

The actual transformation matrix of O_{P2} coordinate system relative to OO_R coordinate system is: Δx_{p2}, Δy_{p2}, Δz_{p2}, $\Delta\alpha_{p2}$, $\Delta\beta_{p2}$, $\Delta\gamma_{p2}$:

$$\begin{cases} T_{04p}' = \begin{bmatrix} 1 & -\Delta\gamma_{P2} & \Delta\beta_{P2} & \Delta x_{P2} \\ \Delta\gamma_{P2} & 1 & -\Delta\alpha_{P2} & \Delta y_{P2} \\ -\Delta\beta_{P2} & \Delta\alpha_{P2} & 1 & \Delta z_{P2} \\ 0 & 0 & 0 & 1 \end{bmatrix} \\ T_{04s}' = I_{4\times4} \end{cases}. \tag{5}$$

6. O_C coordinate system

According to the previous analysis, there are seven errors in the detection of horizontal axis C: $\delta_x(C)$, $\delta_y(C)$, $\delta_z(C)$, $\varepsilon_x(C)$, $\varepsilon_y(C)$, $\varepsilon_z(C)$, η_{ZC}. Therefore, the actual motion transformation matrix of O_C coordinate system relative to O_{P2} coordinate system is:

$$\begin{cases} T_{45p}' = \begin{bmatrix} 1 & -\eta_{zC} & 0 & 0 \\ \eta_{zC} & 1 & 0 & 0 \\ 0 & 0 & 1 & 0 \\ 0 & 0 & 0 & 1 \end{bmatrix} \\ T_{45s}' = \begin{bmatrix} \cos(C) & -\sin(C) & \varepsilon_y(C) & \delta_x(C) \\ \sin(C) & \cos(C) & -\varepsilon_x(C) & \delta_y(C) \\ -\varepsilon_y(C) & \varepsilon_x(C) & 1 & \delta_z(C) \\ 0 & 0 & 0 & 1 \end{bmatrix} \end{cases}. \tag{6}$$

7. O_J coordinate system

The actual transformation matrix of O_J coordinate system with respect to O_C coordinate system is: Δx_J, Δy_J, Δz_J, $\Delta\alpha_J$, $\Delta\beta_J$, $\Delta\gamma_J$:

$$\begin{cases} T_{56p}' = \begin{bmatrix} 1 & -\Delta\gamma_J & \Delta\beta_J & \Delta x_J \\ \Delta\gamma_J & 1 & -\Delta\alpha_J & \Delta y_J \\ -\Delta\beta_J & \Delta\alpha_J & 1 & \Delta z_J \\ 0 & 0 & 0 & 1 \end{bmatrix}. \\ T_{56s}' = I_{4\times4} \end{cases} \tag{7}$$

8. O_M coordinate system

Due to the installation errors of O_M in calibration Block J: Δx_M, Δy_M, Δz_M, $\Delta\alpha_M$, $\Delta\beta_M$, $\Delta\gamma_M$, the actual transformation matrix of O_M coordinate system relative to O_J coordinate system is:

$$\begin{cases} T_{67p}' = \begin{bmatrix} 1 & -\Delta\gamma_M & \Delta\beta_M & \Delta x_M \\ \Delta\gamma_M & 1 & -\Delta\alpha_M & \Delta y_M \\ -\Delta\beta_M & \Delta\alpha_M & 1 & \Delta z_M \\ 0 & 0 & 0 & 1 \end{bmatrix}. \\ T_{67s}' = I_{4\times4} \end{cases} \tag{8}$$

Based on the analysis of the actual transformation matrix, the zero-order motion equation of the endoscopic measurement point in O_M can be established as follows:

$$o_w' = \left[T_{04}'T_{45}'T_{56}'T_{67}'\right]^{-1}\left[T_{01}'T_{12}'T_{23}'\right]\cdot o_t \cdot . \tag{9}$$

In Eq. (9), $T'_{ij}=T'_{ijp}\cdot T'_{ijs}$, T'_{ijp} is the transformation matrix of static error, T'_{ijs} is the transformation matrix of motion error.

Due to the influence of geometric error of the detection system, it can be considered that the actual detection point o_w' is the result of the superposition error motion matrix E of the ideal detection point o_w:

$$o_W' = E\cdot o_W . \tag{10}$$

Union Eqs. (1) , (9) , (10) :

$$\begin{cases} o_w = \left[T_{04}T_{45}T_{56}T_{67}\right]^{-1}\left[T_{01}T_{12}T_{23}\right]\cdot o_t \\ o_w' = \left[T_{04}'T_{45}'T_{56}'T_{67}'\right]^{-1}\left[T_{01}'T_{12}'T_{23}'\right]\cdot o_t \cdot . \\ o_W' = E\cdot o_W \end{cases} \tag{11}$$

The error motion matrix E is derived from Eq. (11) and solved by Eq. (12) as follows:

$$E = \left[\left(T_{04}'T_{45}'T_{56}'T_{67}'\right)^{-1}\left(T_{01}'T_{12}'T_{23}'\right)\right]\cdot \cdot\left[\left(T_{04}T_{45}T_{56}T_{67}\right)^{-1}\left(T_{01}T_{12}T_{23}\right)\right]^{-1} \tag{12}$$

Based on the small error assumption, the error motion transformation matrix E can be assumed to be Eq. (13):

$$E = \begin{bmatrix} 1 & -\theta_z & \theta_y & \Delta x \\ \theta_z & 1 & -\theta_x & \Delta y \\ -\theta_y & \theta_x & 1 & \Delta z \\ 0 & 0 & 0 & 1 \end{bmatrix}. \tag{13}$$

In Eq. (13), θ_x, θ_y, θ_z are the orientation errors of the actual detection point of the endoscope relative to the ideal detection point, Δx, Δy, Δz are the position errors of the actual detection point of the endoscope relative to the ideal detection point respectively.

This leads to Eq. (14):

$$\begin{bmatrix} 1 & -\theta_z & \theta_y & \Delta x \\ \theta_z & 1 & -\theta_x & \Delta y \\ -\theta_y & \theta_x & 1 & \Delta z \\ 0 & 0 & 0 & 1 \end{bmatrix} = \left[\left(T_{04}'T_{45}'T_{56}'T_{67}'\right)^{-1}\left(T_{01}'T_{12}'T_{23}'\right)\right]\cdot \cdot\left[T\left(_{04}T_{45}T_{56}T_{67}\right)^{-1}\left(T_{01}T_{12}T_{23}\right)\right]^{-1}. \tag{14}$$

Before testing the inner surface of the main cylinder using the testing system, the installation error of each component of the testing system can be adjusted to a minimum by using a precision calibration tool:

$$\begin{cases} \Delta x_N \approx 0 & \Delta y_N \approx 0 & \Delta z_N \approx 0 & \Delta\alpha_N \approx 0 & \Delta\beta_N \approx 0 & \Delta\gamma_N \approx 0 \\ \Delta x_{P1} \approx 0 & \Delta y_{P1} \approx 0 & \Delta z_{P1} \approx 0 & \Delta\alpha_{P1} \approx 0 & \Delta\beta_{P1} \approx 0 & \Delta\gamma_{P1} \approx 0 \\ \Delta x_{P2} \approx 0 & \Delta y_{P2} \approx 0 & \Delta z_{P2} \approx 0 & \Delta\alpha_{P2} \approx 0 & \Delta\beta_{P2} \approx 0 & \Delta\gamma_{P2} \approx 0 . \\ \Delta x_J \approx 0 & \Delta y_J \approx 0 & \Delta z_J \approx 0 & \Delta\alpha_J \approx 0 & \Delta\beta_J \approx 0 & \Delta\gamma_J \approx 0 \\ \Delta x_M \approx 0 & \Delta y_M \approx 0 & \Delta z_M \approx 0 & \Delta\alpha_M \approx 0 & \Delta\beta_M \approx 0 & \Delta\gamma_M \approx 0 \end{cases} \tag{15}$$

The error components of the testing system can be obtained by calculating the Eq. (14) and bringing Table 2 and the Eqs. (1) – (8) into it, with this method, the detection error of the detection system can be obtained directly, and the accuracy of the detection system can be improved.

5. Error Measurement

On-line measurement of geometric error elements in the measuring system is carried out by using XL -80 laser dual-frequency interferometer. The measuring module of XL -80 is shown in Fig. 6.

5.1. Vertical linear axis error detection

The geometric error of the vertical linear axis Z is measured, and the mean error data is obtained by drawing 3 measurements with MATLAB, as shown in Fig. 7.

The error mean data shown in Fig. 8 are analyzed:

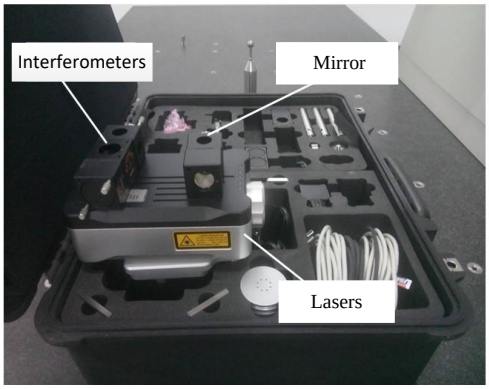

Fig. 6 Measurement component

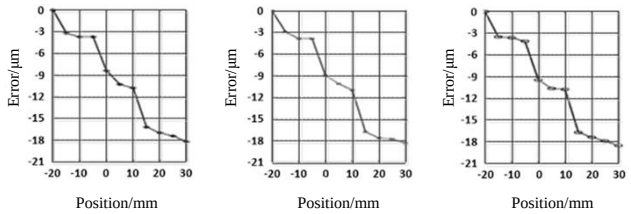

a b c

Fig. 7 Linear axis *Z* error curve: a – the 1st test curve, b – the 2nd test curve, c – the 3rd test curve

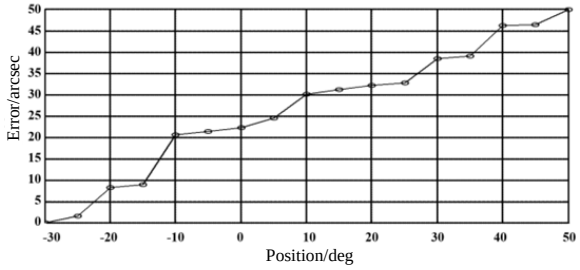

Fig. 8 Error curve of horizontal axis

1. The trend of the three error curves is basically the same;

2. The maximum error is close to 20 μm;

3. The error change has obvious monotonicity. It is concluded that the vertical linear axis *Z* motion has good repeatability and is easy to realize precision compensation.

5.2. Error detection of horizontal rotating shaft

The XL -80 Rotary Axis measurement module is used to measure the *C* geometric error of the horizontal rotary axis of the detection system.

The mean error data shown in Fig. 8 are analyzed as follows:

1. The *C* rotation error of the horizontal axis of rotation has obvious monotonicity;

2. The maximum value of the rotation error is about 50 arcsec. From this, the horizontal axis *C* movement regularity is obvious, can achieve precision compensation.

5.3. Verticality error detection

The verticality error is measured by using XL -80 verticality measuring module, and the verticality error data is shown in Table 3.

Table 3 is analyzed as follows:

1. The straightness error $\delta_y(z)$, $\delta_x(z)$ of the vertical linear axis Z torsional pendulum are very small;

2. The rotation error $\varepsilon_x(\alpha)$ and deflection error $\varepsilon_y(\alpha)$ of the horizontal axis C are also very small;

3. The verticality error of the vertical linear axis *Z* and the horizontal axis *C* is even smaller. It is shown that the verticality error of vertical linear axis Z and horizontal rotation *C* has little influence on the detection accuracy and can be neglected.

6. Error Compensation Experiment

Based on the error analysis of the testing system, a comprehensive error compensation scheme is designed, whose structure is shown in Fig. 9. The realization process is as follows:

1. Establishing a compensation model to compensate the controlled parameters Δz, $\Delta\theta$;

2. Testing and checking the detection precision of the detection system after compensation, the error compensation model is shown in Eq. (16).

$$\begin{cases} y = -0.2603x + 12.8349 & [20, 25] \\ y = -0.1169x - 20.4461 & [15, 20] \\ y = -0.1317x + 15.5479 & [10, 15] \\ y = -1.1456x - 28.3208 & [5, 10] \\ y = -0.0391x - 11.3321 & [0, 5] \\ y = -0.2148x - 8.7930 & [-5, 0] \\ y = -1.0863x - 3.8121 & [-10, -5] \\ y = -0.0623x - 3.8121 & [-15, -10] \\ y = -0.0391x - 3.5370 & [-20, -15] \\ y = -0.7856x + 11.7939 & [-25, -20] \end{cases} . \quad (16)$$

Fig. 10 shows a sectional view of the structure of the sample under test, and Table 4 shows the data before and after compensation for the sample under test.

An analysis of Table 4 shows that:

1. For the diameter data of 1 and 2 compensating holes of the standard sample, the measured data before and after the compensation are the same, and the diameter parameters of the main brake cylinder have little relation with the geometric error of the measuring system, which is mainly affected by the image processing technology.

2. According to the position data of the compensation hole 1 of the standard sample, the detection result of the

Table 3

Verticality error data

Node	Vertical linear axis, μm		Horizontal axis of rotation, deg		Verticality error, deg
	$\delta_y(z)$	$\delta_x(z)$	$\varepsilon_x(\alpha)$	$\varepsilon_y(\alpha)$	
1	0.4814	0.5742	0.0031	0.0045	0.0012
2	1.0236	1.2534	0.0052	0.0087	0.0014
3	1.2515	2.0097	0.0084	0.0141	0.0023
4	2.0311	2.5743	0.0131	0.0183	0.0031
5	2.6583	3.3643	0.0160	0.0211	0.0046
6	3.1154	4.5809	0.0197	0.0290	0.0069
7	3.3432	4.8099	0.0231	0.0299	0.0058
8	4.1741	5.3476	0.0269	0.0341	0.0064
9	4.7967	6.4325	0.0290	0.0332	0.0072
10	5.3565	7.0098	0.0323	0.0423	0.0076

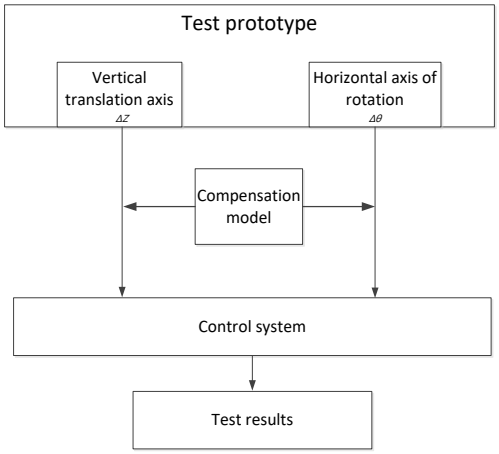

Fig. 9 Error compensation structure diagram

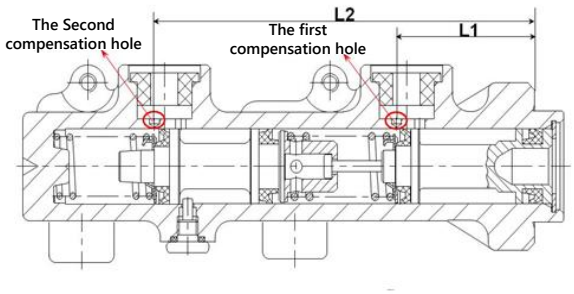

Fig. 10 Inspection sample section view

Table 4
Analysis of test data before and after compensation

Test items		Part number	ZDZG-22.2-12.3851/mm
Standard sample data	Compensation hole ①	Diameter	0.7±0.125
		Position	71.03±0.1
	Compensation hole ②	Diamete	0.7±0.125
		Position	85.19±0.1
Data before compensation	Compensation hole ①	Diamete	0.675
		Position	71.130
	Compensation hole ②	Diamete	0.708
		Position	85.080
Data after compensation	Compensation hole ①	Diamete	0.675
		Position	71.086
	Compensation hole ②	Diamete	0.708
		Position	85.142

detection system has reached the standard before the compensation, which shows that the position data of the compensation hole 1 is less affected by the geometric error of the detection system because of the structural characteristics.

3. According to the position data of the compensation hole 2 of the standard sample, the test result exceeds the set tolerance before compensation, and the test result after compensation is within the controllable range, it shows that the error compensation method can effectively improve the detection accuracy of the detection system.

7. Conclusions

1. A technical detection scheme for the inner surface of the braking master cylinder integrating light, machine, electricity and calculation is proposed, which improves the accuracy and efficiency of the inner surface of the braking master cylinder and meets the performance requirements of the current industrial background for the detection of the inner surface of the braking cylinder;

2. The multi-body system theory and the principle of homogeneous coordinate transformation in robot kinematics are cited to establish the comprehensive error model of the surface detection system of the braking master cylinder, and the concept of specific error compensation is proposed. The above research is experimentally proved to be able to effectively improve the accuracy of the braking master cylinder detection system;

3. This paper carries out advanced technology research on the current situation of inner surface detection of braking master cylinder, and completes the detection demand of master cylinder in the industrial background, which provides theoretical reference for the modernization transformation of other automobile parts, and also has positive guiding significance for the development of automobile parts technology.

Acknowledgments

This research is from the Science and Technology Research Project of the Education Department of Jilin Province: Research on the Compensation Hole Detection System of the Inner of the Master Cylinder of Automobile Brakes (No. JJKH20210690KJ).

References

1. **Borodin, A. L.; Vasiliev, V. I.; Maltseva, G. I**. 2021. Mathematical diagnostic model of brake master cylinder of hydraulic brake system of automobile, IOP Conference Series: Materials Science and Engineering 1061(1): 012011. https://doi.org/10.1088/1757-899X/1061/1/012011.
2. **Liu, G. X.; Yan, Y. P.; Meng, J.** 2024. Study on the detection technology for inner-wall outer surface defects of the automotive ABS brake master cylinder based on BM-YOLOv8, Measurement Science and Technology 35(5): 055109. https://doi.org/10.1088/1361-6501/AD25DF.
3. **Zhao, C. F.; Ding, H. C.; Cao, G. H.; Hou, H.** 2021. Research on automatic detection technology for the compensation hole shape and position parameters of a brake master cylinder, Advances in Mechanical Engineering 13(7): 1-16. https://doi.org/10.1177/16878140211034616.
4. **Wei, J.; Jiang, L.; Liang, B.** 2024. Geometric error compensation method of five-axis CNC machine tool based on improved genetic algorithm, Journal of Physics: Conference Series 2825(1): 012029. https://doi.org/10.1088/1742-6596/2825/1/012029.
5. **Cheng, Y. B.; Luo, P. H.; Shen, B.; Wang, Y. H.; Li, Y.; Li, S. H.** 2024. Analysis of Long-Distance Geometric Error Measurement and Uncertainty Based on PSD Laser Collimation Principle, Photonics 11(6): 538. https://doi.org/10.3390/photonics11060538.
6. **Liang, S.; Wu, Y.; Hou, L.; Dong, L., Fan, Q. W.; Zhang, H. Y.** 2023. Research on influence mechanism of geometric error sources on tooth surface error of VH-CATT gear special machine tool, The International Journal of Advanced Manufacturing Technology 128(11-12): 5529-5546.

https://doi.org/10.1007/s00170-023-12001-z.
7. **Yao, S. H.; Huang, H. Z.; Tian, W. J. Gao, W. G.; Weng, L.T.; Zhang, D.W.** 2023. Simultaneous identification for geometric error of dual rotary axes in five-axis machine tools, Measurement 220: 113368. https://doi.org/10.1016/j.measurement.2023.113368.
8. **Wu, S.; Yuan, C. Q.; Yu, T.; Wang, Y. P.; Zhang, Y.** 2023. Comprehensive analysis and evaluation of the geometric errors of the rotating axis of five-axis double-pendulum machine tools based on S-shaped samples, The International Journal of Advanced Manufacturing Technology 129(11-12): 5135-5148. https://doi.org/10.1007/s00170-023-12572-x.
9. **Tang, X. X.; Zhou, H. B.; Xu, T. Y.** 2023. A geometric errors identification method for the rotating axis of five-axis welding equipment, International Journal of Precision Engineering and Manufacturing 24(8): 1355-1367. https://doi.org/10.1007/S12541-023-00829-0.
10. **Chen, C.; Wen, C. Y.; Liu, Z.; Xie, K.; Zhang, Y.; Chen, C. L. P.** 2017. Adaptive Consensus of Nonlinear Multi-Agent Systems With Non-Identical Partially Unknown Control Directions and Bounded Modelling Errors, In IEEE Transactions on Automatic Control 62(9): 4654-4659. https://doi.org/10.1109/tac.2016.2628204.

G. L. Wang, B. Yu

THE IMPROVEMENT OF DETECTION PRECISION OF INTERNAL SURFACE DETECTION SYSTEM OF MAIN CYLINDER

S u m m a r y

In view of the current status of the inspection of the main cylinder inner surface of the key components in the automobile brake system, an advanced inspection scheme integrating light, machine, electricity and calculation is put forward, the basic structure and the concrete implementation scheme of the detection system are given, and the geometric error elements are analyzed according to the working principle of the detection system, based on the theory of multi-body system in robot kinematics and the principle of homogeneous coordinate transformation, the comprehensive error model of the detection system was constructed, and the geometric error of the detection system is detected on-line by XL-80 dual-frequency laser interferometer, the existing geometric error data are obtained, the error compensation scheme of the detection system is put forward, and the error compensation verification of the detection system is carried out, it is proved that the proposed method can effectively improve the detection accuracy of the internal surface of the master cylinder.

Keywords: brake master cylinder, inner surface, geometric error, error compensation, accuracy improvement.

Received September 12, 2024
Accepted February 21, 2025